Nanoscale Advances

NIR Luminescence lifetime nanothermometry based on phonon assisted Yb3+-Nd3+ energy transfer

Journal:	*Nanoscale Advances*
Manuscript ID	NA-ART-04-2021-000285.R1
Article Type:	Paper
Date Submitted by the Author:	31-May-2021
Complete List of Authors:	Maciejewska, Kamila; Instytut Niskich Temperatur i Baden Strukturalnych Bednarkiewicz, Artur; Institute of Low Temperature and Structure Research, Polish Academy of Sciences, Excited State Spectroscopy Department; Marciniak, Lukasz; Polish Academy of Sciences, Institute of Low Temperature and Structure Research

NIR Luminescence lifetime nanothermometry based on phonon assisted Yb^{3+}-Nd^{3+} energy transfer

K. Maciejewska[1], A. Bednarkiewicz[1], L. Marciniak[1]

[1]Institute of Low Temperature and Structure Research, Polish Academy of Sciences, Okólna 2, 50-422 Wroclaw, Poland

Corresponding author: l.marciniak@intibs.pl

Keywords: luminescence thermometry, lifetimes, phonon assisted energy transfer, lanthanides, relative sensitivity, orthophosphates, nanocrystals

Abstract

Luminescence thermometry in biomedical sciences is highly desirable, but also highly challenging and demanding technology. Numerous artifacts have been found during steady-state spectroscopy temperature quantification, such as ratiometric spectroscopy. Oppositely, luminescence lifetime is considered as most reliable indicator of temperature thermometry because this luminescent feature is not susceptible to sample properties or luminescence reabsorption by the nanothermometers themselves. Unfortunately, this type of thermometers is much less studied and known. Here, thermometric properties of the Yb^{3+} ions in $Nd_{0.5}RE_{0.4}Yb_{0.1}PO_4$ luminescent temperature probes were evaluated aiming to design and optimize luminescence lifetime based nanothermometers. Temperature dependency of the luminescent lifetimes is induced by thermally activated phonon assisted energy transfer from $^2F_{5/2}$ state of Yb^{3+} ions to the $^4F_{3/2}$ state of Nd^{3+} ions, which in turn is responsible the significant quenching of the Yb^{3+}:$^2F_{5/2}$ lifetime. It was also found, that the thermal quenching and thus

relative sensitivity of luminescent thermometer can be intentionally altered by the RE ions used (RE= Y, Lu, La, Gd). The highest relative sensitivity was found for $Nd_{0.5}Y_{0.4}Yb_{0.1}PO_4$ S_R=1.22%/K at 355K at it remains above 1%/K up to 500K. The high sensitivity and reliable thermometric performance of the $Nd_{0.5}La_{0.4}Yb_{0.1}PO_4$ was confirmed by the high reproducibility of the temperature readout and the temperature uncertainty being as low as δT=0.05 K at 383K.

Introduction

The consistent growth of scientific interest in the luminescent thermometry (LT) - a technique that exploits temperature-induced changes in the luminescent properties of a phosphor for temperature readout, results from the capability of remote thermal imaging that it offers[1–7]. One of the most sophisticated examples of such remote thermal readout is an *in vivo* thermal imaging of the biologic system, where, in a noninvasive and electrically passive manner, information about temperature distribution in the living cells and tissues can be visualized with a submicrometer spatial resolution[6,8–11]. This may not only provide the information about the rate of the biological processes (e.g. thermogenesis) but may also enable feedback-controlled medical treatments (e.g. hyperthermal therapy)[12–14].

The most commonly exploited spectroscopic feature of the thermometric phosphors that, after calibration, reports about temperature is luminescence spectra shape. Most commonly the intensity ratio of two emission bands are used[15–24]. However, because the shape of the emission band may be affected by the unknown and sample-to-sample variable absorption of the medium surrounding the phosphor or by the interparticle interactions within the sample, the credibility of the ratiometric LT approach, especially in the *in vivo* applications, has been recently undermined[25,26]. Although some strategies to mitigate, correct or circumvent these limitations have been recently proposed by involving primary thermometry concept or multiparametrical

luminescent thermometers, this approaches require complicated correction and analysis of the obtained data[27].

An important alternative temperature indicator utilize thermal dependent kinetics of the excited states. Unlike short living fluorophores (e.g. organic dyes, fluorescent proteins, most QDs), the luminescence lifetime of excited states of lanthanides is almost unaffected by the absorption or scattering by the medium and, when the surface of the phosphor is isolated from the surroundings by the optically passive shell, its kinetics is also independent on the local chemical environment. Despite this concept is promising, the relative sensitivity of lifetime-based LT is usually considered as lower with respect to the ratiometric counterpart[5,28–31]. This is because the excited levels kinetics is modified by quenching through temperature dependent multi-phonon processes. Therefore, to boost the sensitivity of luminescence lifetime based LT, the other energy transfer processes susceptible to temperature should be involved.

As it has been recently demonstrated, the energy transfer relaying on the absorption of phonon could be the appropriate direction to follow[32]. Therefore, in this manuscript a comprehensive and detailed investigation on the thermal dependence of phonon mediated energy transfer between Yb^{3+} and Nd^{3+} ions is performed in order to develop a highly sensitive luminescent thermometer based on the kinetics of the Yb^{3+} ions. As the probability of a phonon assisted energy transfer depends on many material parameters of the host, the performed studies have been conducted on the series of $Nd_{0.5}RE_{0.4}Yb_{0.1}PO_4$ (where RE= Y^{3+}, Lu^{3+}, La^{3+}, Gd^{3+}) nanocrystals in order to select the most promising candidate. The proposed phosphate matrix is inherently biocompatible, resistant to strong oxidizing and reducing acids (nitric, hydrochloric acid) and enable easy fine tuning of spectral properties by intentional substitution of RE with numerous optically passive ions (e.g. RE: Y^{3+}, Lu^{3+}, La^{3+}, Gd^{3+} which differ in ionic radius, coordination number etc.). [33–35]

2. Materials and Methods

Materials

The monazite $Nd_{1-x}RE_xPO_4:Yb^{3+}$ nanoparticles (NPs) (RE: Y^{3+}, Lu^{3+}, La^{3+}, Gd^{3+}) were synthesized via precipitation method. All chemicals: ytterbium (III) oxide, Yb_2O_3 (99.99%, Alfa Aesar), europium (III) oxide, Nd_2O_3 (99.9%, Alfa Aesar), yttrium (III) oxide Y_2O_3 (99.99%, Alfa Aesar), lutetium (III) oxide Lu_2O_3 (99.99%, Alfa Aesar), lanthanum (III) oxide La_2O_3 (99.99%, Alfa Aesar) and gadolinium (III) oxide Gd_2O_3 (99.99%, Alfa Aesar) as well as ammonium hydrogen phosphate, $(NH_4)_2HPO_4$ (98.0%, Alfa Aesar) and polyethylene glycol (99.5%, Chempur) were used without further purification.

Synthesis

Stoichiometric amounts of oxides (Y_2O_3, Lu_2O_3, La_2O_3, Gd_2O_3, Nd_2O_3 and Yb_2O_3) were diluted using Teflon-lined autoclave in ultrapure nitrate acid to produce nitrates, followed by evaporation of the excess of the solution and drying over P_2O_5 in a vacuum desiccator for 1 day. The procedure of the synthesis of $Nd_{0.5}RE_{0.4}Yb_{0.1}PO_4$ (where RE: Y^{3+}, Lu^{3+}, La^{3+}, Gd^{3+}) nanoparticles contain two steps. The first step consisted of the precipitation of orthophosphates in polyethylene glycol and water solution using $(NH_4)_2HPO_4$ water solution (0.17 mol/L) at 50^{o}C. In the second step, the slurry was centrifuged and washed three times in water and ethanol. Obtained orthophosphates were aged in 80^{o}C for 12h and after that was annealed at 900^{o}C for 2h to obtain the powders.

Methods

Powder diffraction studies were carried out using a PANalytical X'Pert Pro diffractometer equipped with an Anton Paar TCU 1000 N Temperature Control Unit using Ni-filtered Cu Ka radiation (V= 40 kV, I= 30 mA). Transmission electron microscopy images were obtained using a FEI Tecnai G2 20 X-TWIN microscope supplied with a CCD FEI Eagle 2K camera with a

HAADF detector and electron gun with a LaB_6 cathode. The pattern presented on the left side of the TEM images is the microscope artifact.

The FLS1000 spectrometer from Edinburgh Instruments equipped with a R928P side window photomultiplier tube from a Hamamatsu detector, was used to carry out measurements of photoluminescence decay curves and excitation spectra utilizing a micro-flash lamp and a halogen lamp, respectively. The emission spectra were measured using Silver-Nova Super Range TEC Spectrometer from Stellarnet of 1 nm spectral resolution and 808 nm excitation lines from an laser diode. The excitation pulse duration was modulated using simple electronic PWM system. The thermal dependencies of both emission spectra and luminescence decay profiles were measured using THMS 600 heating-cooling stage from Linkam (0.1 °C temperature stability and 0.1 °C set point resolution) to control the temperature.

3.Results and discussion

Although the RE orthophosphates crystalizes in a three different crystallographic structures (tetragonal, monoclinic and hexagonal) due to the ionic size of the Nd^{3+} ions the $NdPO_4$ crystalizes in the monazite-type monoclinic structure of $P2_1/c$[14] symmetry and following unit parameters: a=6.4537 Å, b=7.0425 Å, c=8.2012 Å, β=125.8328°. In this case the $[PO_4]$ - $[REO_x]$ - $[PO_4]$ chains are interlinked with 9 oxygen ions (Fig. 1a)[36]. The nine-fold coordinated site of the Nd^{3+} ions of C_1 point symmetry can be successfully substituted by the RE ions because of the similarity in the ionic radii. The phase purity of the synthesized nanocrystals has been confirmed by the powder X-ray diffraction pattern measurements. All of the observed diffraction reflexes correspond to the reference pattern (ICSD 61262). However, due to the difference in the ionic radii between the substituting RE and Nd^{3+} ions, and in consequence a change of the unit cell parameters, the shift of the diffraction peaks can be observed. The values of the cell parameters obtained from the Rietveld refinement method has been listed in Table 1. It can be clearly seen that for the $Nd_{0.5}RE_{0.4}Yb_{0.1}PO_4$ nanocrystals, the cell volume increases

according to the following order: $V_{Y3+}<V_{Lu3+}<V_{Gd3+}<V_{La3+}$. As was confirmed by the TEM studies, the synthesized powders consist of the aggregated nanocrystals (Figure 1c-f, see also FIG S 1). The diameter of the nanocrystals is affected by the type of the RE cation used, reached d=40±12 nm for Y^{3+}; d=55±10 nm for Lu^{3+}; d=60±10 nm for La^{3+} and d=32±12 nm for Gd^{3+} (Fig. S2). In the case of Raman spectra, most of the recorded bands are characteristic for the vibrations of the phosphate groups (i.e. P–O symmetric stretching, P–O asymmetric stretching, and O–P–O symmetric/asymmetric bending vibrations). However, all the modes are shifted toward higher energies in a sequence $La^{3+} < Y^{3+} < Lu^{3+} < Gd^{3+}$ (dashed area in the spectra).

Table 1. The calculated structural parameters of $Nd_{0.5}RE_{0.4}Yb_{0.1}PO_4$ nanocrystals based on the XRD patterns

RE^{3+}	Crystal structure	Point symmetry	Max phonon energy (cm^{-1})	a	b	c	Cell volume ($Å^3$)	Ionic radius of RE (Å) [coordination number]
Lu	monoclinic	C_1	1071	6.35179	6.85549	8.01249	348.90	1.019 [8]
Y	monoclinic	C_1	1063	6.37804	6.87694	8.03117	352.26	0.977 [8]
La	monoclinic	C_1	1060	6.44380	6.98207	8.17155	367.65	1.216 [9]
Gd	monoclinic	C_1	1072	6.36476	6.88189	8.04216	352.26	1.107 [9]

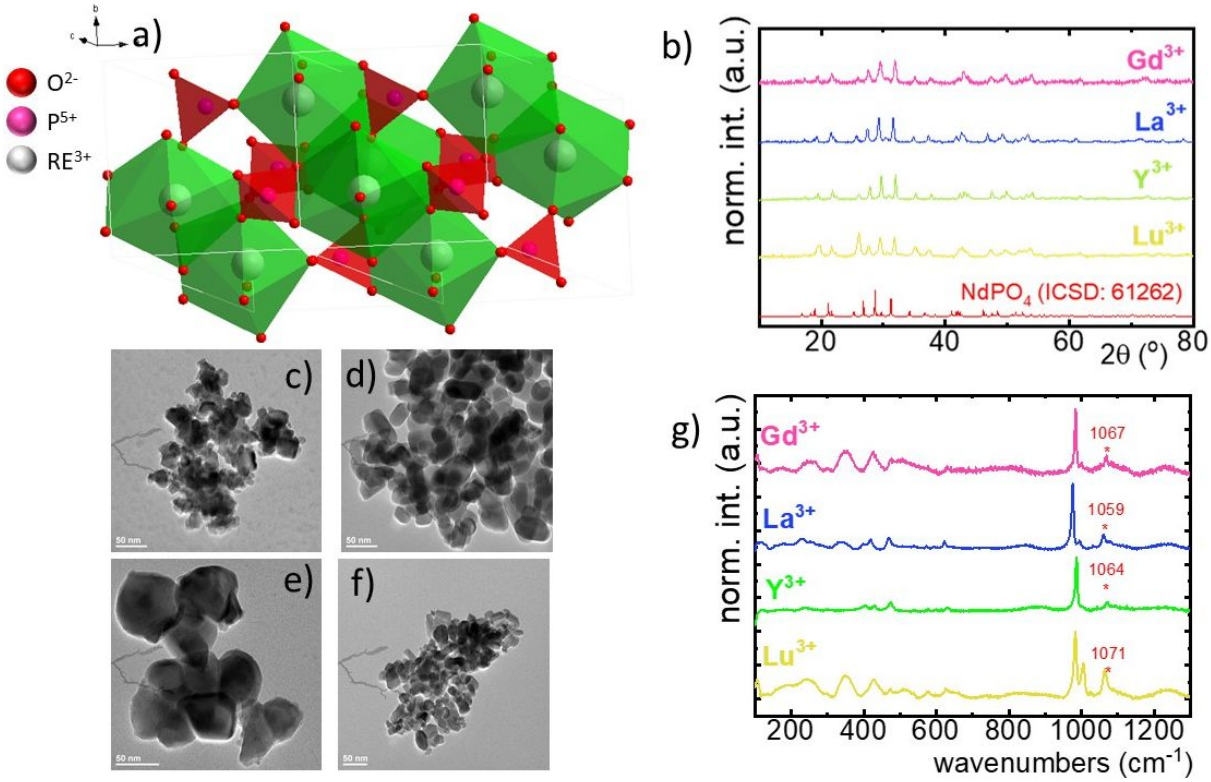

Figure 1. The visualization of the double cell unit of $NdPO_4$ structure (a); X-ray diffraction patterns of $Nd_{0.5}La_{0.4}Yb_{0.1}PO_4$, $Nd_{0.5}Y_{0.4}Yb_{0.1}PO_4$, $Nd_{0.5}Lu_{0.4}Yb_{0.1}PO_4$and , $Nd_{0.5}Gd_{0.4}Yb_{0.1}PO_4$ (b). The representative TEM mages of $Nd_{0.5}La_{0.4}Yb_{0.1}PO_4$ (c), $Nd_{0.5}Y_{0.4}Yb_{0.1}PO_4$ (d), $Nd_{0.5}Lu_{0.4}Yb_{0.1}PO_4$ (e) and, $Nd_{0.5}Gd_{0.4}Yb_{0.1}PO_4$ (f) nanocrystals; the comparison of the Raman spectra for $Nd_{0.5}RE_{0.4}Yb_{0.1}PO_4$nanocrystals (g).

In order to explain the luminescent properties of the $Nd_{0.5}Lu_{0.5}PO_4$:Yb^{3+} nanocrystals, simplified energy level diagrams of Nd^{3+} and Yb^{3+} ions are presented in Figure 2a. As can be found, Yb^{3+} energy level scheme is relatively simple and consists only of two energy levels- $^2F_{7/2}$ ground state and $^2F_{5/2}$ excited state. Therefore, upon λ_{exc}=940 nm photoexcitation, which corresponds to the energy difference between those two states, only single emission band of Yb^{3+} at λ_{exc}=980 nm can be observed. The relatively large energy gap between those two states leads to the low probability of the nonradiative $^2F_{5/2}$ state depopulation via multiphonon processes. On the other hand, Nd^{3+} ions are characterized by the more abundant energy state configuration. The radiative depopulation of the excited metastable $^4F_{3/2}$ state leads to the occurrence of the three emission bands usually localized at around 880 nm, 1060 nm and 1350 nm attributed to the $^4F_{3/2}\rightarrow{}^4I_{9/2}$, $^4F_{3/2}\rightarrow{}^4I_{11/2}$ and $^4F_{3/2}\rightarrow{}^4I_{13/2}$, respectively. The fact that the $^4F_{3/2}$

energy level is localized roughly 900 cm^{-1} above the $^2F_{5/2}$ state of Yb^{3+} ions allows for the energy transfer between these ions which however must be accompanied by the absorption of the host phonon. According to the Miyakava-Dexter theorem, the probability of the interionic energy transfer $W_{ET}(T)$ is expressed by the following formula[37–40]:

$$W_{ET}(T) = W_0 e^{-\beta \Delta E} \left(\frac{1}{e^{\frac{\Delta E}{kT}} - 1} \pm 1 \right)^N \quad (1)$$

where W_0, β, ΔE, k, T and N parameters represent the energy transfer probability at perfect energy match between the interacting ions, a material parameter, energy gap between interacting energy levels, Boltzmann constant, temperature in Kelvins and the number of phonons involved in the process, respectively. At elevated temperatures, energy from the Yb^{3+}:$^2F_{5/2}$ state can be transferred to the Nd^{3+}:$^4F_{3/2}$ state with the absorption of the phonon, which will lead to the quenching of the $^2F_{5/2} \rightarrow {}^2F_{7/2}$ Yb^{3+} luminescence and is manifested as intensity dimming and shortening of the Yb^{3+}:$^2F_{5/2}$ lifetime. The opposite energy transfer from Nd^{3+} to Yb^{3+} may also occur, but in this case the emission of phonon is more probable as compared to the phonon absorption. The confirmation of the Nd^{3+} to Yb^{3+} energy transfer is the appearance of the characteristic absorption bands of the Nd^{3+} associated with the *4f-4f* electronic transition in the excitation spectra monitored for the emission of Yb^{3+} ions λ_{em}=980 nm (Figure 2b). Besides the Nd^{3+} absorption band, one of the most intense absorption band in the recorded excitation spectra is located at 940 nm which shall be associated with the $^2F_{7/2} \rightarrow {}^2F_{5/2}$ transition of Yb^{3+} ions. Moreover, the $Nd^{3+} \rightarrow Yb^{3+}$ energy transfer is confirmed by the presence of Yb^{3+}:$^2F_{5/2} \rightarrow {}^2F_{7/2}$ emission band under λ_{exc}=808 nm optical excitation, which corresponds to the $^4I_{9/2} \rightarrow {}^4F_{5/2}$, $^2H_{9/2}$ electronic transition of Nd^{3+} ions. The excitation and emission spectra (Fig. 2b and c) does not reveal any significant differences for different $Nd_{0.5}RE_{0.5}PO_4$: Yb^{3+} nanocrystals. The comparison of the integral emission intensities of the Yb^{3+} luminescence associated with the $^2F_{5/2} \rightarrow {}^2F_{7/2}$ electronic transition measured at room temperature reveals that

$Nd_{0.5}Gd_{0.5}PO_4$: Yb^{3+} emits twice brighter than $Nd_{0.5}La_{0.5}PO_4$: Yb^{3+} and $Nd_{0.5}Y_{0.5}PO_4$: Yb^{3+} and even 5 times brighter than $Nd_{0.5}Lu_{0.5}PO_4$: Yb^{3+} (Fig. S5).

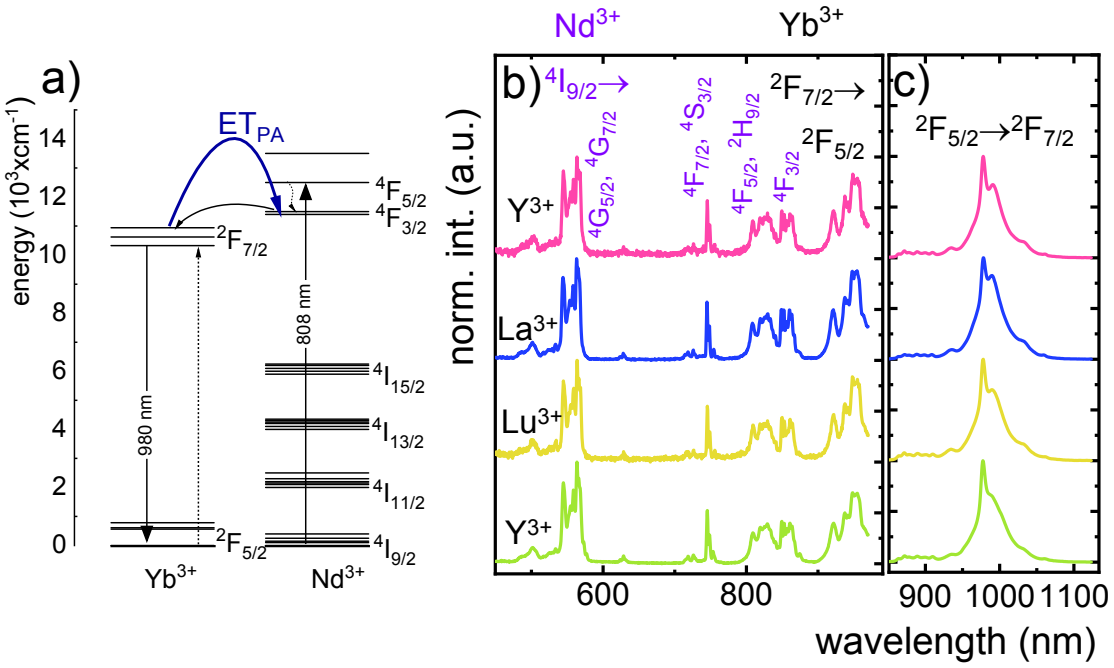

Figure 2. The schematic simplified energy level diagram of Yb^{3+} and Nd^{3+} ions in $Nd_{0.5}RE_{0.4}Yb_{0.1}PO_4$ (a), comparison of the normalized excitation spectra monitored at the emission of Yb^{3+} ions λ_{em}=980 nm (b) and emission spectra upon λ_{exc}=808 nm (c) for different $Nd_{0.5}RE_{0.4}Yb_{0.1}PO_4$ nanocrystals

The technical feasibility and accuracy of lifetime-based remote temperature determination can be improved when the lifetime of the emitting center is relatively long and strongly thermally dependent, respectively. The feasibility of this methods gains from efficient phosphors, which can be easily photoexcited with cheap, powerful and all-electronically controlled laser diodes, while detection of long (μs-ms) kinetics can be easily detected with current Si based photosenors equipped with simple (in opposite to digitizers of sub ns – ns lifetimes) digital oscilloscope based fluorescence acquisition. Moreover, in the case of some specific

applications, such as thermal bioimaging, longer luminescence decays enable temporal separation of the luminescence of the thermal probe from the background emission (i.e. autofluorescence) of the tissue. Additionally, boosting the sensitivity of the thermal probe to temperature changes becomes easily available, because the probability of the energy transfer with the absorption of the phonon (eq.1) is strongly dependent on temperature. Therefore, luminescent thermometer that involves this process is expected to possess favorable thermometric properties. The probability W_0 depends on the spatial distance between the interacting ions. Therefore, in order to enhance the probability of the phonon assisted energy transfer, shortening of the Nd^{3+} to Yb^{3+} distance is desired. As it has already been reported by many authors, an increase of the Yb^{3+} concentration leads to the enhancement of the quenching of the Yb^{3+} luminescence via the migration of the energy among excited states of Yb^{3+} to the quenching centers[41,42]. It is especially acute in the case of the nanosized phosphors for which the distance to the particle surface is relatively low. Therefore, in order to avoid the activation of this quenching channel the concentration of Nd^{3+} ions has been increased in this work. As it can be seen, initially, for low Nd^{3+} concentration, the probability of phonon assisted energy transfer was relatively low what is confirmed by relatively small changes of the $^2F_{5/2}$ lifetime at elevated temperatures (Fig. S3). An increase of the Nd^{3+} amount up to 50% results in significant thermal quenching of the $^2F_{5/2}$ state, which results from the phonon-assisted energy transfer from Yb^{3+} to Nd^{3+} ions being facilitated by short distance between interacting ions. These results may suggest that further increase of the Nd^{3+} concentration should be beneficial for the thermometric performance. However, the increase of the Nd^{3+} concentration leads to the shortening of the initial lifetime value (measured at 83 K) what may hinder the luminescence kinetics measurement at higher temperatures. Therefore, in order to satisfy the conditions of long luminescence lifetime and strong thermal dependence of the luminescence lifetime of $^2F_{5/2}$ state, the concentration of 50% of Nd^{3+} seems to be optimal. It must be noted here, that the

luminescence lifetime values themselve determine and actually limit the temporal resolution of temperature imaging in general. Therefore, although long luminescence lifetimes simplify technical means to detect and record the signal, they may concurrently limit the capabilities to image fast and dynamic processes. The phonon assisted energy transfer between Yb^{3+} and Nd^{3+} ions leads to the significant quenching of the Yb^{3+} luminescence which is reflected by the lowering of the $^2F_{5/2} \rightarrow {}^2F_{7/2}$ emission intensity (Fig. 3a, see also Fig. S4), which reached 50% of its initial intensity at around 0°C. Moreover, the shape of the emission band was slightly changed what can be associated with the thermalization of the higher laying Stark components of the $^2F_{5/2}$ state at elevated temperature. As presented in Fig. 3b, the luminescence decay profile of Yb^{3+} ions significantly changes in this temperature range (see also Fig. S6 and Fig. S7). Notably, an in-depth analysis of the obtained decay profiles reveals the short rise-time which is associated with the $Nd^{3+} \rightarrow Yb^{3+}$ energy transfer. Due to the fact that at higher temperature the profiles slightly deviate from the exponential decay, the average lifetime of the excited states has been calculated as follows:

$$\tau_{avr} = \frac{A_1\tau_1^2 + A_2\tau_2^2}{A_1\tau_1 + A_2\tau_2} \quad (2)$$

The analysis of the thermal dependence of τ_{avr} indicates that the RE^{3+} ions significantly affect the rate and the temperature of the activation of the thermal quenching of the $^2F_{5/2}$ luminescence. The initial (at 110 K) τ_{avr} decreases from τ_{avr} =0.31 ms for La^{3+}, τ_{avr} =0.29 ms for Y^{3+}, τ_{avr} =0.22 ms for Lu^{3+} to τ_{avr} =0.12 ms for Gd^{3+}. This dependence may be associated both with the interionic distance between neighbor Nd^{3+} and Yb^{3+} ions (which is dependent on the ionic radii of the RE^{3+} ions) and the phonon energy of the host material. It can also be noticed that the value of the rise times is also affected by the host material composition. In the case of the $Nd_{0.5}Y_{0.4}Yb_{0.1}PO_4$, when the temperature increases, thermal quenching of the $^2F_{5/2}$ state instantly initializes. On the other hand, the quenching process started around 200 K for

$Nd_{0.5}La_{0.4}Yb_{0.1}PO_4$ and $Nd_{0.5}Y_{0.4}Yb_{0.1}PO_4$. The highest thermal susceptibility reveals $Nd_{0.5}Gd_{0.4}Yb_{0.1}PO_4$ for which τ_{avr} starts to decreases above 220 K. In the case of all the host materials under investigation, the most significant τ_{avr} changes can be observed in the 200-400 K temperature range. In order to quantify the quenching process, the temperature at which τ_{avr} reached half of its initial value (T_{50}) was considered (Figure 3f). As can be seen, the T_{50} increases as follows T_{50}=256K (Y^{3+}), T_{50}=295K (Lu^{3+}), T_{50}=303K (La^{3+}) and T_{50}=320K (Gd^{3+}). Similar trend was reported previously by Witkowski et al.[43] for $REPO_4:Ce^{3+}$ (the stars in the Fig. 3f). Although thermal quenching process in this case was discussed in terms of electron transfer to the conduction band, similar trend and influence of the host material was observed in the case of the Nd^{3+},Yb^{3+} co-doped systems.

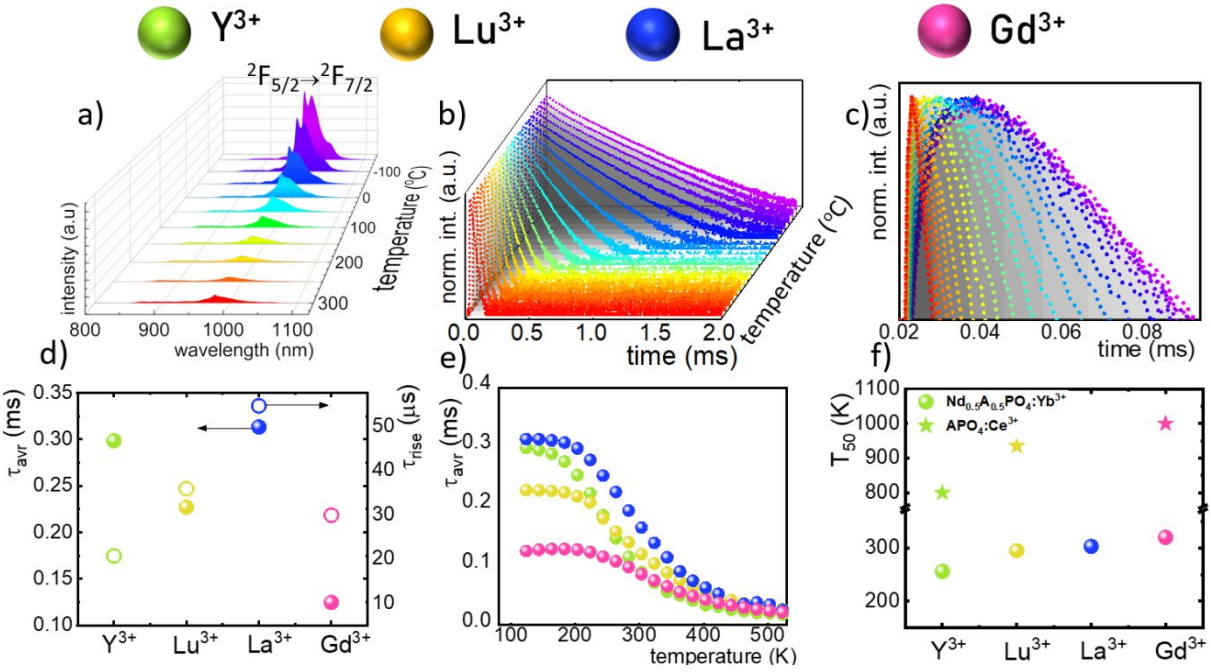

Figure 3. Thermal evolution of the emission spectra of $Nd_{0.5}Y_{0.4}Yb_{0.1}PO_4$ nanocrystals (a) and luminescence decay profile of $^2F_{5/2}$ state of Yb^{3+} ions (b); thermal evolution of the rise times (c); The colours on (a)-(c) correspond to each other. The comparison of the decay times and rise times measured at 110 K (d) and thermal

evolution of the τ_{avr} (e) for different host materials; the T_{50} parameter for $Nd_{0.5}RE_{0.4}Yb_{0.1}PO_4$ (dots) and $REPO_4:Ce^{3+}$ (stars) (f).

One of the most important thermographic parameters that enables to directly compare thermometric performance of different luminescent thermometer is relative thermal sensitivity S_R which, in the case of average luminescence lifetime used as thermometric parameter, is defined as follows:

$$S_R = \frac{1}{\tau_{avr}} \frac{\Delta \tau_{avr}}{\Delta T} 100\% \quad (3)$$

where $\Delta \tau_{avr}$ corresponds to the change of τ_{avr} at ΔT change of temperature. In the case of the $Nd_{0.5}RE_{0.4}Yb_{0.1}PO_4$ nanocrystals, the S_R increases at elevated temperatures reaching its maximal local value above 350 K (Figure 4a). The highest S_R=1.22 %/K was found for $Nd_{0.5}Y_{0.4}Yb_{0.1}PO_4$, while S_R=1.05%/K for $Nd_{0.5}La_{0.4}Yb_{0.1}PO_4$, S_R=0.85 %/K for $Nd_{0.5}Lu_{0.4}Yb_{0.1}PO_4$ and S_R=0.74 %/K for $Nd_{0.5}Gd_{0.4}Yb_{0.1}PO_4$ (Figure 4b). The temperature at which S_R reached its maximal value increases from T_{SRMAX}=355 K for $Nd_{0.5}Y_{0.5}PO_4:Yb^{3+}$ up to 445 K $Nd_{0.5}Gd_{0.4}Yb_{0.1}PO_4$ (Figure 4c). It needs to be mentioned here, that despite the fact the S_{RMAX} for $Nd_{0.5}Gd_{0.4}Yb_{0.1}PO_4$ was found at higher temperature, the values of S_R for $Nd_{0.5}Y_{0.4}Yb_{0.1}PO_4$ exceeds the sensitivities of the other host materials in the entire analysed temperature range. The rate of the quenching of $^2F_{5/2}$ state of Yb^{3+} ions can be also evaluated by the analysis of the absolute sensitivity (S_A):

$$S_A = \frac{\Delta \tau_{avr}}{\Delta T} \quad (4)$$

The maximal S_A=1.65 μs/K was found for the $Nd_{0.5}Y_{0.4}Yb_{0.1}PO_4$. According to the expectations, the temperature at which the maximal value of S_A was reached correlates well

with the T_{50} temperature (Figure 3f). It should be emphasized that in the case of the nanosized phosphors their spectroscopic properties such as the shape of the emission spectra, luminescence lifetime and the ultimately thermometric properties may depend on the size of the nanoparticles. However, no such correlation could be found versus the series of passive Ln^{3+} dopants (Y^{3+}, La^{3+}, Gd^{3+}, Lu^{3+}) used in our studies (Figure S8). Moreover it was found that the τ_{avr} is in principle independent on the emission wavelength used when the 950-980 nm spectral rage is used (Figure S9). However at λ_{em} =990 nm a slightly longer value of the lifetime was found. This effect may be also related with the small difference in the crystallographic surrounding of some Yb^{3+} ions localized in the $REPO_4$ nanocrystals (different crystallographic sites). This may modify the probabilities in the nonradiative depopulation rates of the $^2F_{5/2}$ states and since the contribution of the emission intensity of Yb^{3+} ions from different crystallographic sites depends on the spectral range, the lifetime may in consequence slightly vary with the detection wavelength used.

In order to verify the thermal stability of the synthesized nanocrystals and the repeatability of temperature readout based on the lifetime of the $^2F_{5/2}$ state of the Yb^{3+} ions, the luminescence decay profiles were measured in a several heating-cooling cycles (Figure 4e). The obtained results confirm good thermometric performance of the $Nd_{0.5}RE_{0.4}Yb_{0.1}PO_4$ luminescent thermometers. Additionally the thermal determination uncertainty (δT) was calculated as follows:

$$\delta T = \frac{1}{S_R}\frac{\delta\tau_{avr}}{\tau_{avr}} \quad (5)$$

where $\delta\tau_{avr}$ represents the uncertainty of the lifetime determination (in our case this parameter was determined as a standard deviation from 10 luminescence decay profile measurements at constant temperature). In the case of $Nd_{0.5}RE_{0.4}Yb_{0.1}PO_4$ above 350K, all host materials revealed superior thermometric performance with the δT below 0.1 K. However, for the

$Nd_{0.5}Y_{0.4}Yb_{0.1}PO_4$, the $\delta T<0.1K$ was obtained for temperatures above 273K with the minimal uncertainty $\delta T=0.05$ K at 383K. To determine whether the duration of the excitation pulse affects the τ_{avr} the luminescence decay profiles of $Nd_{0.5}Y_{0.4}Yb_{0.1}PO_4$ nanocrystals were measured as a function of pulse width modulation (Figure S10). However no pulse duration effect was found in this case. The presented results confirm that the $Nd_{0.5}Y_{0.4}Yb_{0.1}PO_4$ exhibit most favourable kinetics based thermometric performance from all the studied materials. It needs to be noted that the additional nonradiative quenching processes associated with ligands attached to the nanoparticle surface may reduce the emission intensity and reduce the susceptibility of the Yb^{3+} lifetimes to temperature variations. Therefore, as recently proposed the Chen et al.[32], the passivation of the nanoparticle surface by optically inactive shell layer may improve the thermometric properties of such thermographic phosphor. Thus the relative sensitivity of 1.4%/K at 283K was achieved for $NaYF_4$@$NaYF_4$:Yb^{3+},Nd^{3+}@CaF_2 [32]

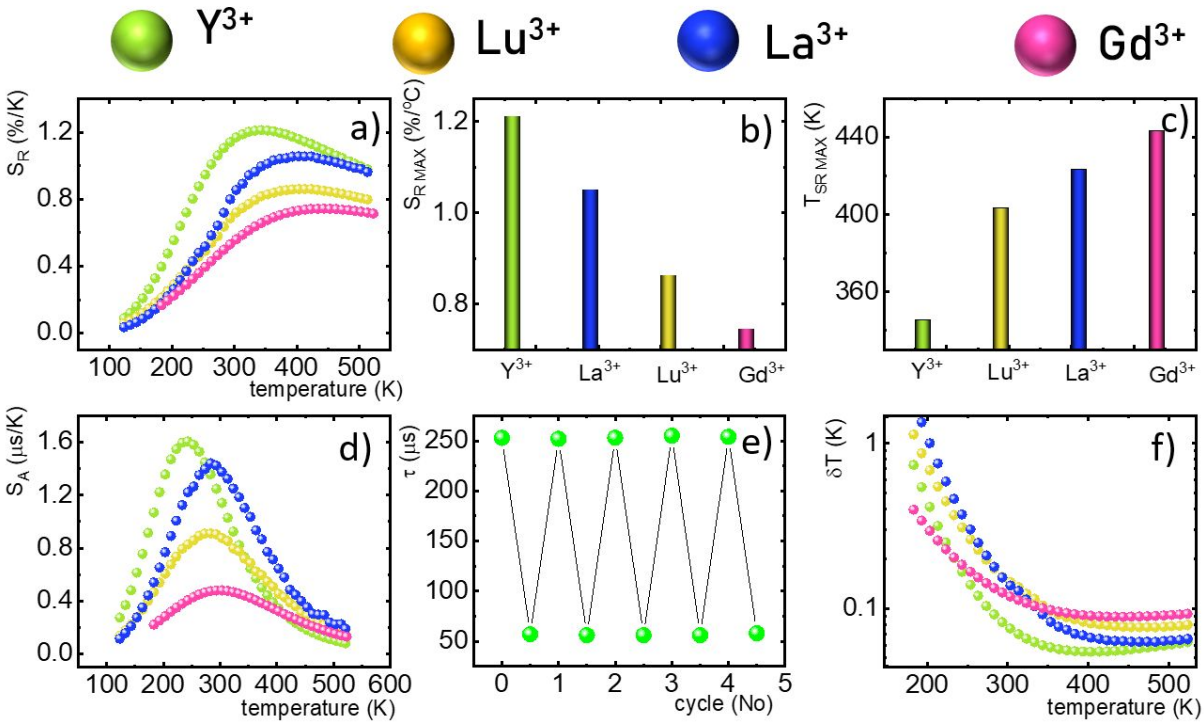

Figure 4. Thermal evolution of the S_R for $Nd_{0.5}RE_{0.4}Yb_{0.1}PO_4$ (a); the comparison of the S_{RMAX} (b) and T_{SRMAX} (c) for different $Nd_{0.5}RE_{0.4}Yb_{0.1}PO_4$; the comparison of the S_A at different temperatures (d); the lifetime of the

$^2F_{5/2}$ state in $Nd_{0.5}Y_{0.4}Yb_{0.1}PO_4$ in several heating-cooling cycles (e); δT calculated as a function of temperature (f).

Conclusions

The thermometric performance of the Yb^{3+} luminescence lifetime based thermometers in $Nd_{0.5}RE_{0.4}Yb_{0.1}PO_4$ nanocrystals was investigated in a wide temperature range. Temperature dependent phonon assisted energy transfer from $^2F_{5/2}$ excited state of Yb^{3+} to the $^4F_{3/2}$ state of Nd^{3+} ions was proposed as the thermal sensitivity mechanism. The influence of the temperature on the τ_{avr} was investigated for different RE ions (RE=Y, Lu, La, Gd). It was found that for the optimal concentration of 50% Nd^{3+} ions at elevated temperatures, the luminescence lifetime of the Yb^{3+}:$^2F_{5/2}$ state was rapidly quenched. The determined temperature, at which luminescence lifetime reached half of its initial value (T_{50}), increases from T_{50}=256K (Y^{3+}) through T_{50}=295K (Lu^{3+}), T_{50}=303K (La^{3+}) to T_{50}=320K for Gd^{3+} passive co-dopants. High thermal quenching of the thermometric parameter (i.e. the lifetime of the Yb^{3+}:$^2F_{5/2}$ state) is reflected in the thermometric performance of described remote temperature probe. The highest absolute and relative sensitivities were found for the $Nd_{0.5}Y_{0.4}Yb_{0.1}PO_4$ compound – i.e. S_A=1.65 μs/K at 225K and S_R=1.22%/K at 355K were obtained, respectively. The change of the RE ions decreases the maximal value of the S_R and increases the temperature at which S_{RMAX} is reached. High thermometric performance of the $Nd_{0.5}Y_{0.4}Yb_{0.1}PO_4$ phosphor was also confirmed by good repeatability of the lifetime readout within many heating-cooling cycles and by low temperature determination uncertainty (δT=0.05 K at 383K). The obtained results indicate that the phonon assisted energy transfer should be considered in further works as a promising mechanism that may boost the sensitivity of lifetime based remote temperature probes.

Acknowledgements

The financial support from the European Union's Horizon 2020 FET Open program under grant agreement no. 801305 is acknowledged.

References

1 M. Dramićanin, in *Woodhead Publishing Series in Electronic and Optical Materials*, ed. M. B. T.-L. T. Dramićanin, Woodhead Publishing, 2018, pp. 1–12.

2 J. Zhou, B. del Rosal, D. Jaque, S. Uchiyama and D. Jin, *Nature Methods*, 2020, **17**, 967–980.

3 A. Bednarkiewicz, L. Marciniak, L. D. Carlos and D. Jaque, *Nanoscale*, 2020, **12**, 14405–14421.

4 X. Wang, O. S. Wolfbeis and R. J. Meier, *Chemical Society Reviews*, 2013, **42**, 7834–7869.

5 L. D. Carlos and F. Palacio, *Thermometry at the Nanoscale*, The Royal Society of Chemistry, 2016.

6 D. Jaque and F. Vetrone, *Nanoscale*, 2012, 4301–4326.

7 M. Suta and A. Meijerink, *Advanced Theory and Simulations*, **n/a**, 2000176.

8 C. D. S. Brites, A. Millán and L. D. Carlos, *Handbook on the Physics and Chemistry of Rare Earths*, 2016, **49**, 339–427.

9 D. Chrétien, P. Bénit, H.-H. Ha, S. Keipert, R. El-Khoury, Y.-T. Chang, M. Jastroch, H. T. Jacobs, P. Rustin and M. Rak, *PLOS Biology*, 2018, **16**, e2003992.

10 S. Arai, M. Suzuki, S.-J. Park, J. S. Yoo, L. Wang, N.-Y. Kang, H.-H. Ha and Y.-T. Chang, *Chemical Communications*, 2015, **51**, 8044–8047.

11 S. Kiyonaka, R. Sakaguchi, I. Hamachi, T. Morii, T. Yoshizaki and Y. Mori, *Nature Methods*, 2015, **12**, 801–802.

12 E. Carrasco, B. del Rosal, F. Sanz-Rodríguez, Á. J. de la Fuente, P. H. Gonzalez, U. Rocha, K. U. Kumar, C. Jacinto, J. G. Solé and D. Jaque, *Advanced Functional Materials*, 2015, **25**, 615–626.

13 E. Hemmer, P. Acosta-Mora, J. Méndez-Ramos and S. Fischer, *J. Mater. Chem. B*, 2017, **5**, 4365–4392.

14 B. del Rosal, E. Carrasco, F. Ren, A. Benayas, F. Vetrone, F. Sanz-Rodríguez, D. Ma, Á. Juarranz and D. Jaque, *Advanced Functional Materials*, 2016, **26**, 6060–6068.

15 M. Dramićanin and B. Windows, *Biomedical Applications of Luminescence Thermometry*, 2018.

16 M. D. Dramićanin, *Luminescence Thermometry*, Elsevier, 2018.

17 M. Sekulić, V. Đorđević, Z. Ristić, M. Medić and M. D. Dramićanin, *Advanced Optical Materials*, 2018, **6**, 1–7.

18 M. Suta, Ž. Antić, V. Đorđević, S. Kuzman, M. D. Dramićanin and A. Meijerink, *Nanomaterials*, 2020, **10**, 543.

19 L. Marciniak, A. Bednarkiewicz, D. Kowalska and W. Strek, *Journal of Materials Chemistry C*, , DOI:10.1039/C6TC01484D.

20 K. Maciejewska and L. Marciniak, *Chemical Engineering Journal*, 2020, **402**, 126197.

21 K. Kniec, M. Tikhomirov, B. Pozniak, K. Ledwa and L. Marciniak, *Nanomaterials*, 2020, **10**, 1–12.

22 C. Matuszewska, K. Elzbieciak-Piecka and L. Marciniak, *Journal of Physical Chemistry C*, 2019, **123**, 18646–18653.

23 A. M. Kaczmarek, M. K. Kaczmarek and R. Van Deun, *Nanoscale*, 2019, **11**, 833–837.

24 O. A. Savchuk, J. J. Carvajal, C. D. S. Brites, L. D. Carlos, M. Aguilo and F. Diaz, *Nanoscale*, 2018, **10**, 6602–6610.

25 L. Labrador-Páez, M. Pedroni, A. Speghini, J. García-Solé, P. Haro-González and D. Jaque, *Nanoscale*, 2018, **10**, 22319–22328.

26 Y. Shen, J. Lifante, N. Fernández, D. Jaque and E. Ximendes, *ACS Nano*, 2020, **14**, 4122–4133.

27 Y. Shen, H. D. A. Santos, E. C. Ximendes, J. Lifante, A. Sanz-Portilla, L. Monge, N. Fernández, I. Chaves-Coira, C. Jacinto, C. D. S. Brites, L. D. Carlos, A. Benayas, M. C. Iglesias-de la Cruz and D. Jaque, *Advanced Functional Materials*, 2020, **n/a**, 2002730.

28 K. Elzbieciak-Piecka, J. Drabik, D. Jaque and L. Marciniak, *Physical Chemistry*

Chemical Physics, 2020, **22**, 25949–25962.

29 S. Arai, S. Lee, D. Zhai, M. Suzuki and Y. T. Chang, *Scientific Reports*, 2014, **4**, 2–7.

30 L. Marciniak, K. Elzbieciak-Piecka, K. Kniec and A. Bednarkiewicz, *Chemical Engineering Journal*, 2020, **388**, 124347.

31 M. D. Chambers and D. R. Clarke, *Annual Review of Materials Research*, 2009, **39**, 325–359.

32 M. Tan, F. Li, N. Cao, H. Li, X. Wang, C. Zhang, D. Jaque and G. Chen, *Small*, 2020, **16**, 2004118.

33 K. Maciejewska, B. Poźniak, M. Tikhomirov, A. Kobylińska and L. Marciniak, *Nanomaterials (Basel, Switzerland)*, 2020, **10**, 421.

34 M. Runowski, A. Shyichuk, A. Tymiński, T. Grzyb, V. Lavín and S. Lis, *ACS Applied Materials & Interfaces*, 2018, **10**, 17269–17279.

35 K. Riwotzki, H. Meyssamy, A. Kornowski and M. Haase, *The Journal of Physical Chemistry B*, 2000, **104**, 2824–2828.

36 W. O. Milligan, D. F. Mullica, G. W. Beall and L. A. Boatner, *Inorganica Chimica Acta*, 1982, **60**, 39–43.

37 T. Miyakawa and D. L. Dexter, *Phys. Rev. B*, 1970, **1**, 2961–2969.

38 S. González-Pérez, I. R. Martín, F. Rivera-López and F. Lahoz, *Journal of Non-Crystalline Solids*, 2007, **353**, 1951–1955.

39 M. O. Ramirez, D. Jaque, L. E. Bausá, I. R. Martín, F. Lahoz, E. Cavalli, A. Speghini and M. Bettinelli, *Journal of Applied Physics*, 2005, **97**, 93510.

40 Ł. Marciniak, A. Bednarkiewicz, M. Stefanski, R. Tomala, D. Hreniak and W. Strek, *Phys. Chem. Chem. Phys.*, 2015, **17**, 24315–24321.

41 F. T. Rabouw, P. T. Prins, P. Villanueva-Delgado, M. Castelijns, R. G. Geitenbeek and A. Meijerink, *ACS Nano*, 2018, **12**, 4812–4823.

42 A. Pilch, C. Würth, M. Kaiser, D. Wawrzyńczyk, M. Kurnatowska, S. Arabasz, K. Prorok, M. Samoć, W. Strek, U. Resch-Genger and A. Bednarkiewicz, *Small*, 2017, **13**, 1701635.

43 D. Witkowski and D. A. Rothamer, *Applied Physics B*, 2017, **123**, 226.